

Water Resources Research

RESEARCH ARTICLE

10.1029/2020WR027618

The Transfer and Transport of a Passive Scalar Within an Isolated Array of Circular Cylinders in a Uniform Flow

Christian Klettner¹ 

¹Department of Mechanical Engineering, University College London, London, UK

Key Points:

- The passive scalar transfer and transport in an array of circular cylinders was investigated
- The mean transfer from the group was found to increase with increasing solid fraction, reach a maximum around $\phi = 0.2$, and then decrease
- A semiempirical analytical model was used to predict the transfer from individual cylinders and the group, with good agreement

Correspondence to:

C. Klettner,
ucemkle@ucl.ac.uk

Citation:

Klettner, C. (2020). The transfer and transport of a passive scalar within an isolated array of circular cylinders in a uniform flow. *Water Resources Research*, 56, e2020WR027618. <https://doi.org/10.1029/2020WR027618>

Received 31 MAR 2020

Accepted 19 AUG 2020

Accepted article online 8 SEP 2020

Abstract The transfer and transport of a passive scalar T from an isolated array of circular cylinders of varying Reynolds number ($Re = [100, 333]$) and solid fraction ($0.0023 < \phi < 0.3$) in a uniform steady flow are investigated. This problem is an abstraction of the flow past emergent vegetation or marine aquaculture, in which passive contaminants are continuously generated. The upstream flow ($T_\infty = 0$) is uniform and incident on an array of N_c cylinders whose surfaces are set to $T_s = 1$. Three-dimensional numerical simulations were carried out to investigate the mean and fluctuating Nusselt number of the individual cylinders and the array as a whole. To help interpret the numerical results a mathematical model, partly based on empirical relationships, is developed to predict the transfer. The transfer of the scalar from the array was found to increase when the Reynolds number was increased. As the solid fraction is increased the transfer increases, reaches a maximum, and then decreases. This is due to the collective effect of all the cylinders resulting in (i) a modification of the incident flow and (ii) a reduction in the scalar gradient between the cylinder surface and the locally incident flow on individual cylinders. These effects are highly dependent on the solid fraction. Additional simulations were carried out to decompose the contribution of these two processes on the transfer of individual cylinders.

1. Introduction

Many environmental and industrial applications involve the flow past solid bodies which are in close proximity, including urban landscapes (Davidson et al., 1995), coastal vegetation (Li et al., 2019; Nepf, 1999), and flow through and around fisheries (Wu et al., 2014). The collective effect of the bodies can have a significant impact on the mean flow through and around the region influencing the transport of any passive scalars continuously generated therein; this is the case in urban areas (e.g., pollutants), emergent vegetation (e.g., contaminants/nutrients), and fisheries (e.g., waste/feces). Particularly for marine aquaculture, which is a rapidly expanding part of some economies (e.g., Canada, Food and Agriculture Organization, 2016), the hazards posed by waste on the local environment have been highlighted (Bannister et al., 2016). A better understanding of these flows and transport processes will help in the management of these sensitive ecosystems (Black, 2001). The common approach of approximating these isolated regions with an array of circular cylinders is applied here (Chang & Constantinescu, 2015; Taddei et al., 2016).

The two important processes for these flows are the effect of the array on the mean flow and secondly, how is the passive scalar transported within the array. Both of these have been extensively studied separately and will be reviewed here. The effect of an isolated body on the upstream and downstream flow is well documented (Batchelor, 1967). For viscous flows past bluff bodies the dipole moment is greater than the inviscid prediction due to the separation of the boundary layer, and this difference can be related to the drag coefficient (Hunt & Eames, 2002). For arrays of bodies, the flow will decelerate in front of and diverge around the array, thereby decreasing the volume flux through it (Belcher et al., 2003). This upstream adjustment region was found to scale with the width of the canopy and was not influenced by the parameter $C_D ab$, where C_D is the drag coefficient of the array, b is the canopy width, and a is frontal area per unit volume of the canopy (Rominger & Nepf, 2011). Nicolle and Eames (2011) used a point force model which included blocking and drag (with a dipole and source term respectively) to predict the flow upstream and within an isolated array of circular cylinders of varying solid fraction. Analytical predictions of the forces on individual cylinders (correlated to the local Reynolds number) were compared to direct numerical simulations to $Re = 100$ and agreement was good. Chang and Constantinescu (2015) carried out large eddy numerical simulations

at $Re = 10,000$ to investigate the flow and turbulence structures of a uniform flow past an array with varying solid fraction.

Forced convection past cylinders has received a lot of attention due to practical applications such as flow in heat exchangers and nuclear reactors, including flow past a single cylinder (Chen et al., 2017; Matsumura & Antonia, 1993) and tandem (side-by-side) cylinders (Zhou et al., 2002) with a Reynolds number range from $Re = 2,500$ – $5,800$. For the flow and geometrical properties considered in this work, the closest previous study is the numerical simulations by Mahir and Altac (2014) which considered the effect of having tandem cylinders (one cylinder directly upstream of another) on the transfer properties at $Re = 100$ and $Re = 200$. For these parameters the mean Nusselt number for an isolated cylinder was $\bar{Nu} \approx 5.2$. For a separation distance $s/D < 4$, vortex shedding from the upstream cylinder was suppressed. When $s/D = 2$, the downstream cylinder's transfer was $\bar{Nu} \approx 2$, while the transfer from the upstream cylinder was also decreased to $\bar{Nu} \approx 4.7$, with zero fluctuation in either cylinder's Nusselt number. However, for $s/D > 4$, there was vortex shedding from the upstream cylinder resulting in a peak fluctuation of the downstream cylinder's Nusselt number of 10% (of \bar{Nu}) for $s/D = 5$. This fluctuation in the Nusselt number then decreased for larger s/D . When $s/D = 10$ the upstream cylinder had the Nusselt number of an isolated cylinder; however the transfer from the downwind cylinder was $\bar{Nu} \approx 4.2$. In the context of flow past coastal vegetation there has been a lot of work decomposing the coefficient of lateral dispersion of a scalar, K_{yy} , which is referred to as the effective scalar diffusivity in this work (Nepf, 1999; Tanino & Nepf, 2008; White & Nepf, 2003). The dominant contributions to K_{yy} at low and high solid fractions were found to be turbulent diffusion and the spatially inhomogeneous flow field due to downstream cylinders respectively (Tanino & Nepf, 2008).

The gap identified in the literature review is an investigation into the effect of Reynolds number and solid fraction on the passive scalar transfer and transport from an isolated array of circular cylinders. The major difference between flow past cylinders in a confined channel and an isolated array of cylinders is that in a confined channel there are two lengthscales which need to be taken into account, namely, the size of the cylinder and the distance between the cylinders. For the isolated arrays considered in this study, there is an additional lengthscale, the effective diameter of the group. It is anticipated that as the Reynolds number is increased that the transfer from the array is increased; however the effect of varying the solid fraction is not so clear, because as the number of cylinders is increased, the transfer of the passive scalar will increase. However, as the number of cylinders is increased there will be an increased effect on the flow upstream of the array, resulting in a decreased volume flux through the array, resulting in a lower local Reynolds number for downstream cylinders. Additionally, the gradient of the passive scalar adjacent to the cylinder surface will decrease due to cylinders sitting in the wake of upstream cylinders.

The paper is structured as follows: In section 2 the problem is defined and the governing equations are presented. The numerical methodology is described in section 3. In section 4 a mathematical model is developed for estimating the passive scalar transfer from an array of cylinders. In section 5 the numerical results are analysed in detail and compared to the mathematical model where possible. Conclusions are given in section 6.

2. Problem Definition and Governing Equations

The arrays of varying solid fraction ϕ are composed of N_c cylinders which are each $L = 10D$ long, where D is the diameter of the individual cylinders and are located in a circular region of constant area ($= \pi D_G^2/4$). Figure 1 shows a schematic of the problem and the properties of the arrays are summarized in Table 1. The origin of the Cartesian coordinate system is at the center of the array at (with the spanwise direction, \hat{z} , pointing into the page). The Reynolds numbers ($Re = U_\infty D/\nu$, where ν is the fluid kinematic viscosity and U_∞ is the uniform incident flow speed) considered in this work are $Re = 100$ and $Re = 333$ which are representative of Reynolds numbers in coastal vegetation (Nepf, 1999).

The fluid is modeled using the incompressible Navier-Stokes equations:

$$\nabla \cdot \mathbf{u} = 0, \quad (1)$$

and

$$\rho \left(\frac{\partial \mathbf{u}}{\partial t} + (\mathbf{u} \cdot \nabla) \mathbf{u} \right) = -\nabla p + \nabla \cdot \boldsymbol{\tau}, \quad (2)$$

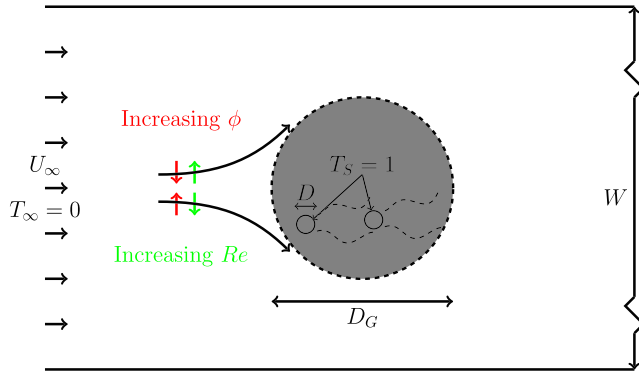


Figure 1. A schematic of the computational domain, of width $W = 38D_G$, is shown with the region (constant diameter D_G) of varying solid fraction ϕ (dark gray). The inlet is a uniform flow and $T_\infty = 0$. The array is comprised of N_c cylinders (with the cylinder surfaces set to $T_S = 1$) of diameter $D = D_G/21$ and length $L = 10D$ (see Table 1 for properties of all the arrays considered in this study). The origin of the Cartesian coordinate system is at the center of the array (with \hat{z} pointing into the page). The qualitative effect of increasing ϕ or Re on the streamlines bounding the array are shown.

where ρ is the fluid density, \mathbf{u} is the velocity field, p is the pressure and $\boldsymbol{\tau}$ is the Newtonian viscous stress tensor. The transport of a passive scalar, T , is given by the advection-diffusion equation

$$\frac{\partial T}{\partial t} + \nabla \cdot (\mathbf{u}T) = \nabla \cdot (\alpha \nabla T), \quad (3)$$

where the scalar diffusivity α is a constant and the Prandtl number ($Pr = \nu/\alpha$) was taken to be unity. The local Nusselt number is defined as

$$Nu_\theta = \frac{D}{(T_S - T_\infty)} \frac{\partial T}{\partial n}, \quad (4)$$

where n is the normal vector into the surface of the cylinder, S , and the associated Nusselt number is

$$Nu = \frac{1}{\pi DL} \int_S Nu_\theta dS. \quad (5)$$

The total Nusselt number for the group of cylinders is

$$Nu_G = \left(\frac{D}{D_G} \right) \sum_{i=1}^{N_c} Nu_i, \quad (6)$$

where the subscript i denotes the i th cylinder. Similarly, the group drag coefficient is defined as

$$C_{DG} = \frac{\sum_{i=1}^{N_c} \mathbf{F}_i \cdot \hat{\mathbf{x}}}{\frac{1}{2} \rho U_\infty^2 D_G L}, \quad (7)$$

where \mathbf{F}_i is the force on the i th cylinder. Time averaged quantities are indicated with an overbar (i.e., \bar{C}_{DG} and $\bar{N}u_G$).

3. Numerical Methods

Numerical simulations were carried out with the open-source CFD toolbox OpenFOAM using a finite volume method (Weller et al., 1998). Three-dimensional unstructured meshes were generated in GMSH (Geuzaine & Remacle, 2009). The solver used was icoFoam, and no turbulence modeling was used which is appropriate for the relatively low Reynolds numbers considered in this work. The maximum Reynolds number for the simulations was chosen such that it was significantly above the threshold where there are only the two flow regimes identified by Chang and Constantinescu (2015) present, while still being able to adequately resolve all the time and length scales of the flow. The finest mesh resolution in the boundary layer adjacent to the solid cylinders was $\Delta/D = 0.01$ for the cases with $Re = 333$. The local Reynolds numbers in the arrays ($>N_{39}$) is much smaller than the free stream Reynolds number, resulting in a lower resolution requirement within the array. In the vertical direction there were 60 grid points, which all together resulted in mesh sizes of up to 29 million cells for the arrays with $Re = 333$. Mesh independence was confirmed by performing an additional simulation of N_1 with double the resolution and the force (coefficients and Strouhal numbers) and transfer (Nusselt number) statistics on the single body agreed within 2%. Further

Table 1
The Solid Fraction $\phi = (D/D_G)^2 N_c$ of the Arrays Is Varied by Varying the Number of Cylinders (N_c) in a Region of Constant Area

Number of cylinders (N_c)	N_1	N_7	N_{20}	N_{39}	N_{64}	N_{95}	N_{133}
Solid fraction (ϕ)	0.0023	0.0159	0.0454	0.0884	0.1451	0.2154	0.3016
Distance between cylinders (s/D)	N/A	8	5.5	4	3	2	1.5

information about the mesh independence and validation study is presented in Appendix A1. The time step used was $\Delta t = 0.0005D_G/U_\infty$.

To minimize the influence of the finite computational domain (inlet, sides, and outlet), the array was situated in the middle of a square of side $38D_G$. This gives a blocking ratio of $D_G/W = 0.03$ which ensures that the channel walls have negligible effect (Kumar & Mittal, 2006). The boundary conditions imposed on the computational domain are $U_\infty \hat{x}$ on the inlet surface, kinematic, and no-slip conditions on the rigid cylinders, a slip condition on the lateral side walls (which equates to zero flux through the boundary and zero shear stress at the boundary) and a constant pressure constraint on the outlet. Periodic boundary conditions were used in the spanwise direction, which is appropriate for these types of flows (Chang & Constantinescu, 2015). The Dirichlet boundary condition for the inlet and cylinders was $T_\infty = 0$ and $T_S = 1$, respectively. The initial condition through out the domain was $T = 0$.

To provide an upper limit on the passive scalar transport, potential flow calculations were also carried out. The simulations were initialized and the transient was flushed out which can take up to ≈ 50 convective time units for the higher solid fraction arrays ($\tau = tU_\infty/D_G$). After this point the transfer and transport of the passive scalar was included.

4. Mathematical Model

To help interpret the results of the numerical simulations a mathematical model, consisting of two components, was developed. Firstly an estimate of the mean flow field is made which is then used to estimate the transfer and transport of the passive scalar of the individual components of the array. A leading order description of the velocity field of a freestream velocity of U_∞ incident on an array of N_c circular cylinders (diameter D) was given in Nicolle and Eames (2011) as

$$\begin{aligned} \mathbf{u}(x, y) = & \underbrace{U_\infty(1, 0)\hat{x}}_{\text{uniform}} + \sum_{i=1}^{N_c} \left(\underbrace{\frac{Q_i(x - x_i, y - y_i)}{2\pi((x - x_i)^2 + (y - y_i)^2)}}_{\text{source}} + \right. \\ & \underbrace{\frac{\mu_i}{2\pi} \frac{(-(x - x_i)^2 + (y - y_i)^2, -2(x - x_i)(y - y_i))}{((x - x_i) + (y - y_i)^2)^2}}_{\text{dipole}} \\ & \left. \underbrace{-(1, 0)H(x - x_i) \frac{Q_i}{\sqrt{4\pi\nu_e(x - x_i)/U_\infty}} \exp\left(\frac{-(y - y_i)^2 U_\infty}{4\nu_e(x - x_i)}\right)}_{\text{wake}} \right) \hat{x}, \end{aligned} \quad (8)$$

where $\{x_i, y_i\}$ are the coordinates of the i th cylinder (with the origin in the center of the array). $Q_i = 1/2\bar{C}_{Di}DU_\infty$, $\mu_i = 1/2\mathbf{u}(x_i)\pi D^2$ and \bar{C}_{Di} are the downstream volume flux, dipole moment, and mean drag coefficient of the i th cylinder, respectively, and ν_e is the effective momentum diffusivity. The velocity field at the i th cylinder's location is estimated (as if the cylinder were removed) and the associated local Reynolds number $Re_i = |\mathbf{u}(x_i)|D/\nu$ is calculated. The local Reynolds number can be used to estimate the mean drag coefficient on each cylinder using the correlations ($\bar{C}_{Di} = f(Re_i)$) given in Clift, Grace, and Weber (1978, p. 381) and determine the cylinder Nusselt number (based on an incident flow of $T_\infty = 0$) using the correlation given in Churchill and Bernstein (1977),

$$\bar{N}u = 0.3 + \frac{0.62Re_i^{1/2}Pr^{1/3}}{[1 + (0.4/Pr)^{2/3}]^{1/4}} \left[1 + \left(\frac{Re_i}{282000} \right)^{5/8} \right]^{4/5}. \quad (9)$$

For cylinders which are downstream of other cylinders, the locally incident flow might have a passive scalar value, $T \neq 0$. As the scalar gradient between the cylinder surface and the incident flow is decreased, there is a decreased transfer. An estimate of the passive scalar downstream of the N_c cylinders is

$$T(x, y) = \sum_{i=1}^{N_c} H(x - x_i) T_0 \left(\frac{1}{4\pi\alpha_e(x - x_i)/U_\infty} \right)^{1/2} \times \exp\left(-\frac{U_\infty(y - y_i)^2}{4\alpha_e(x - x_i)} \right), \quad (10)$$

where $H(x - x_i) = 0$ for $(x - x_i) < 0$ and 1 for $(x - x_i) > 0$ which is a superposition of the solution for the steady-state advection diffusion equation from a single point source (Fischer et al., 1979). α_e , referred to as the lateral dispersion coefficient, K_{yy} , by Tanino and Nepf (2008) is the effective scalar diffusivity. Similar to estimating the velocity field, the scalar value is estimated at a cylinder center using (10) and if it is nonzero, the cylinder Nusselt number is calculated by interpolating the estimated value of T between $T = 0$ (\bar{Nu} given by 9) and $T \geq 1$ ($\bar{Nu} = 0$). By summing all these contributions it is possible to estimate the Nusselt number of the individual cylinders and thereby, of the transfer from the group. As $T = 1$ at $(x - x_i)/D = 0.5$, then $T_0 = 2\pi\alpha_e D/U_\infty$. (8) and (10) need to be solved iteratively to ensure that the effect of the wake of upstream cylinders modifies the transfer of the downstream cylinders.

It remains to set values for the effective momentum and scalar diffusivity in (8) and (10). For the low solid fraction arrays, the interaction between the individual wakes and the downstream cylinders is not significant and so it is appropriate to use $v_e = v$ for $Re = 100$ (White & Nepf, 2003). For $Re > 200$ wakes behind cylinders are turbulent (Eames et al., 2011) and therefore for $Re = 333$ the effective viscosity was set to $v_e = 5v$ (White & Nepf, 2003). For low solid fraction arrays setting $\alpha_e = 2v_e$ is appropriate (Hinze, 1975). However, for the high solid fraction arrays ($N_c = 95$ and 133) the lateral dispersion coefficient will be significantly increased by downstream cylinders such that $\alpha_e = 2v_e$ is not appropriate and the choice of α_e is dependent on the pore Reynolds number $Re_s = U_p s/v$, where s is the distance between the cylinders (see Table 1) and

$$U_p = \frac{Q}{D_G(1 - \phi)}, \quad (11)$$

is the pore velocity and Q is the volume flux (per unit length) through the array, which can be normalized as

$$\tilde{Q} = \frac{Q}{D_G U_\infty} = \frac{1}{D_G U_\infty} \int_{-D/2}^{D/2} \bar{u}|_{x=0} dy. \quad (12)$$

For $Re_s > 250$, $K_{yy}/(U_p D)$ was found to be constant (Tanino & Nepf, 2008). For $Re = 100$, the corresponding Re_s was $Re_s|_{N_{95}} = 60$ and $Re_s|_{N_{133}} = 25$ and for $Re = 333$, $Re_s|_{N_{95}} = 250$ and $Re_s|_{N_{133}} = 125$. As such, for the lower Re_s , α_e was interpolated from the Stokes solution by Koch and Brady (1986); for the higher Re_s , α_e was interpolated from Table 3 in Tanino and Nepf (2008).

5. Results

In this section the effect of the Reynolds number and solid fraction on the flow through and around the array and forces on the array are presented. Next, the transfer from the group is investigated and to explain these trends the transfer from individual cylinders is analysed. Finally, additional simulations are carried out to investigate the effect that the locally incident flow and passive scalar characteristics have on the transfer of individual cylinders.

5.1. Flow Through/Around the Arrays

The flow past isolated arrays of cylinders is different to confined flow past cylinders (White & Nepf, 2003) as the flow upstream of the array is decelerated and diverted around the array. As the Reynolds number is increased the viscous component of the drag coefficient decreases resulting in a slight decrease in \tilde{C}_{DG} (see Figure 2a) and the drag coefficient increases monotonically with solid fraction, which is consistent with previous work (Chang & Constantinescu, 2015; Nicolle & Eames, 2011). The integral effect of this drag force is the volume flux through the array increases with Reynolds number and decreases dramatically with solid fraction (Figure 2b). Additional potential flow simulations have been carried out, making it possible to discriminate between inviscid blocking and viscous drag on the volume flux through the array (see figure 10 in Klettner et al., 2019). To highlight the flow diversion around the array for increasing solid fraction, streamline plots (calculated using the mean velocity field) for $N_c = 20, 64$, and 133 are shown in Figure 3, where the red and blue streamlines go through and around the array, respectively.

In Figures 4a and 4d cylinders in the array N_7 behave similar to isolated cylinders. For the arrays with a higher solid fraction, the collective action of the cylinders becomes significant. For example, for N_{39} and $Re = 100$ (Figure 4b), the cylinders have a separation $s/D \approx 4$, which should result in the cylinders at the front of the array undergoing vortex shedding (if it were just two cylinders in tandem, see Sumner, 2010). However, due to the collective action of the cylinders the local Reynolds number is reduced to the point

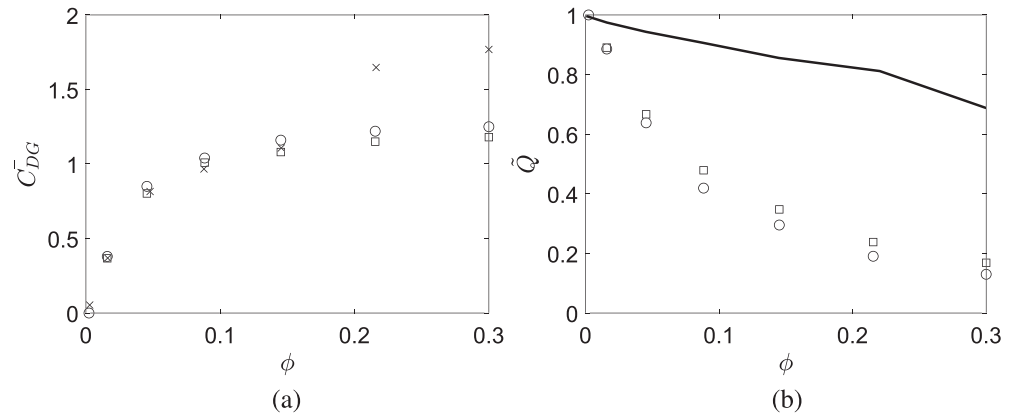


Figure 2. The variation of the (a) time averaged array drag coefficient and (b) normalized volume flux (per unit length) \bar{Q} through the array as a function of solid fraction for $Re = 100$ (\circ) and $Re = 333$ (\square). For reference in (a), the mean drag coefficient for the two-dimensional numerical simulations (at $Re = 100$) in Nicolle and Eames (2011) are shown (\times). The volume flux for a potential flow is given by the solid line in (b).

where there is no vortex shedding. Figure 4e shows that for $Re = 333$, the local Reynolds number is sufficient for the front cylinders of N_{39} to exhibit vortex shedding with a Strouhal number of 0.15, which is reflective of an isolated cylinder at $Re = 80$ (Rajani et al., 2009). For arrays N_{64} , N_{95} , and N_{133} , for both Re considered, the deceleration due to the collective action of the cylinders was sufficient to decrease the incident flow resulting in no vortex shedding from the cylinders at the front of the array (see, e.g., N_{133} in Figures 4c and 4f).

5.2. Scalar Transport/Transfer

5.2.1. Group Transfer

In Figure 5 the mean group Nusselt number \bar{Nu}_G is plotted for (a) $Re = 100$ and (b) $Re = 333$ and as an upper limit, these are compared to potential flow calculations. However, as the solid fraction increases, \bar{Nu}_G increases initially and reaches a peak at $\bar{Nu}_G \approx 7$ and $\bar{Nu}_G \approx 19$ (for $Re = 100$ and $Re = 333$, respectively) for N_{64} after which \bar{Nu}_G decreases. The mathematical model for the low solid fraction arrays (where $\alpha_\epsilon = 2\nu_\epsilon$) works well up to N_{39} (solid line), after which it overpredicts the transfer (Figure 5b). For these lower solid fraction arrays the wakes do not interact significantly and $\alpha_\epsilon = 2\nu_\epsilon$ is a reasonable assumption. However for higher solid fractions the wakes spread far wider due to the downstream cylinders. When α_ϵ is modified to take this into account (Koch & Brady, 1986; Tanino & Nepf, 2008), the reduction in \bar{Nu}_G is captured.

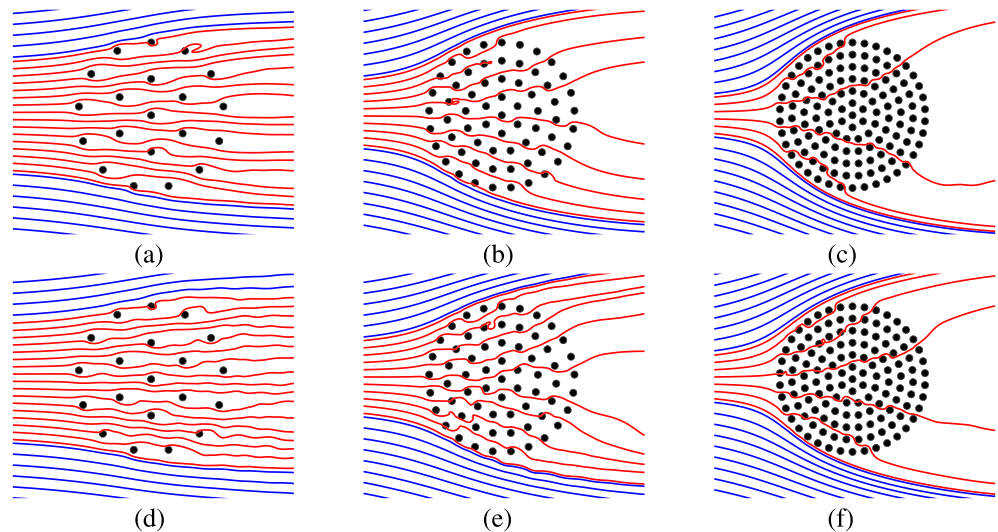


Figure 3. Streamlines of the mean velocity field in the mid plane (at $z/L = 1/2$) for top ($Re = 100$) and bottom row ($Re = 333$) for (a, d) N_{20} , (b, e) N_{64} , and (c, f) N_{133} . The red and blue streamlines go through and around the array respectively. The flow is from left to right.

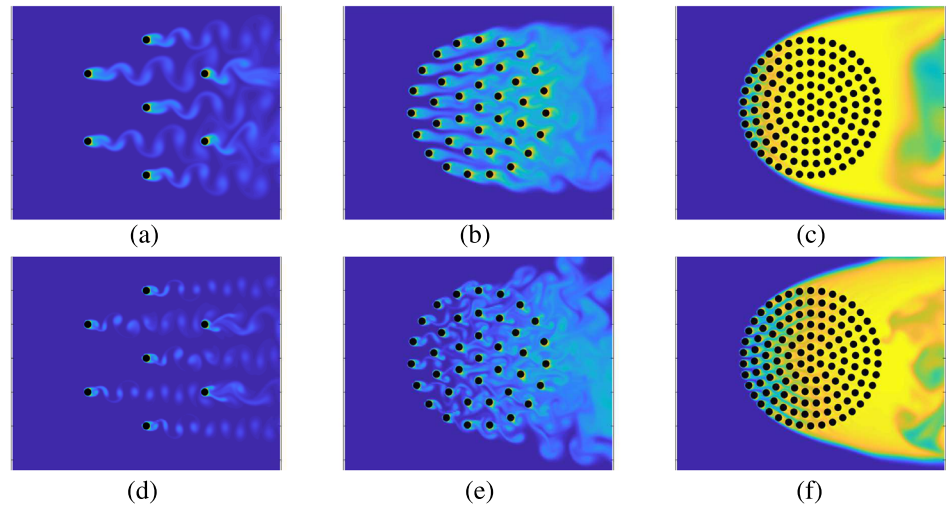


Figure 4. Instantaneous contour plots of the passive scalar field in the midplane ($z/L = 1/2$) for top ($Re = 100$) and bottom row ($Re = 333$) for (a, d) N_7 , (b, e) N_{39} , and (c, f) N_{133} , where $T = 0$ (blue) and $T = 1$ (yellow). The flow is from left to right.

As the Reynolds number is increased \bar{Nu}_G is increased and the potential flow calculations indicate that \bar{Nu}_G increases monotonically and future work could include investigating in what manner finite Reynolds number flows tend to this limit. The Nusselt number of a single cylinder at $Re = 2,100$ (the case of $\phi = 1$ and $D = D_G$) is $\bar{Nu}_G \approx 24$ (Nakamura & Igarashi, 2004). For comparison, the Nusselt numbers for the array N_{133} , for $Re = 100$ and $Re = 333$ are approximately 4 and 16, respectively. Preliminary numerical simulations of the array N_{133} estimate $\bar{Nu}_G = 24$ at $Re \approx 550$. Therefore the transfer of a high solid fraction array is much higher than that of a solid cylinder (for an equivalent Reynolds number). Finally, the fluctuation of the group Nusselt number was low for the Reynolds numbers studied; the highest was 1.7% of \bar{Nu}_G for the array N_{39} at $Re = 333$.

5.2.2. Transfer From Individual Cylinders

Figure 4 shows contour plots of the instantaneous passive scalar with varying Reynolds number and solid fraction, where downstream cylinders are subjected to a steady or unsteady incident flow with possibly $T \neq 0$ (depending on Re and ϕ). As expected, for higher Re , the cylinders have a thinner scalar boundary layer. In Figure 6 a comparison is made between the theoretical model and the numerical simulations for the

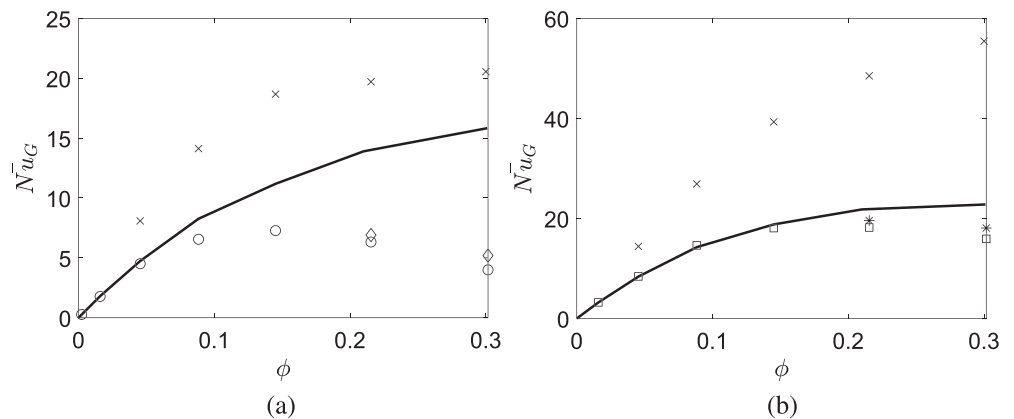


Figure 5. The time averaged group Nusselt number, \bar{Nu}_G , as a function of solid fraction for (a) $Re = 100$ (\circ) and (b) $Re = 333$ (\square). Scalar transport by the potential flow past the array is given by the symbols (\times). The black lines are the analytical prediction for $\alpha_e = 2\nu_e$ while the prediction for high solid fraction arrays using the dispersion coefficients from Koch and Brady (1986) (\diamond) and Tanino and Nepf (2008) ($*$).

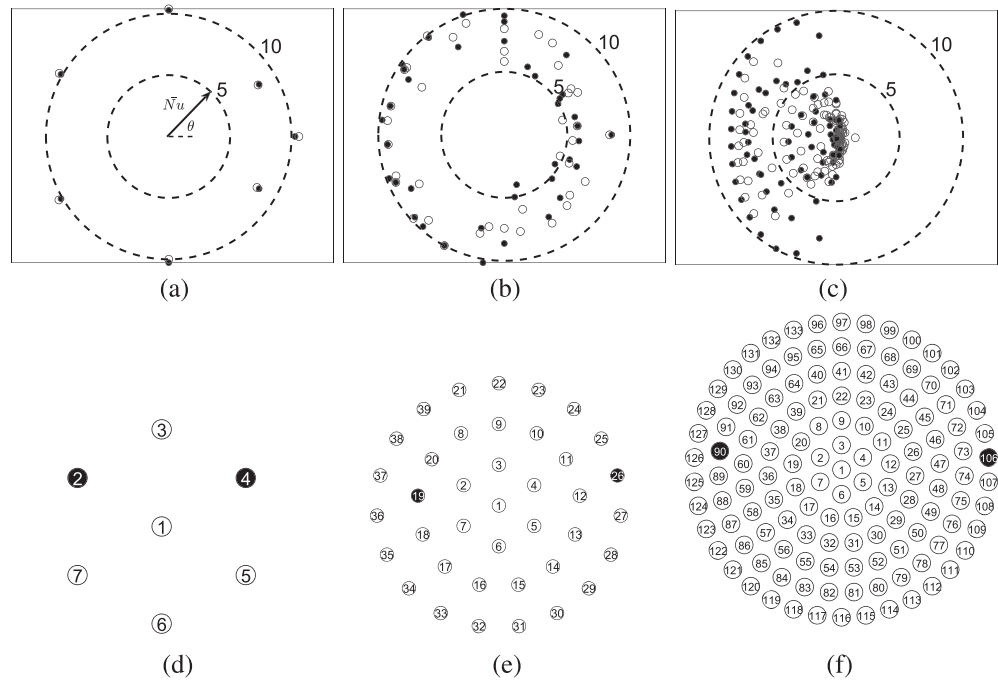


Figure 6. Polar plots of the average Nusselt number of individual cylinders with $Re = 333$ for (a) N_7 , (b) N_{39} , and (c) N_{133} for the numerical simulations (o) and the theoretical predictions $Re = 333$ (•). The angle is $\theta = \tan^{-1}(y_i/x_i)$ and the magnitude is the average Nusselt number. For reference the average Nusselt number for an isolated cylinder at $Re = 333$ is 10.7. The relative positions of the cylinders in the arrays (d) N_7 , (e) N_{39} , and (f) N_{133} are shown. Note: Figures not to scale. The black cylinders are those considered in detail in Figure 7.

mean Nusselt number of the individual cylinders for (a) N_7 , (b) N_{39} , and (c) N_{133} . The results for $Re = 100$ are similar to that of $Re = 333$ and are not shown. For N_7 , there is little interaction between the cylinders and the analytical predictions are quite good, with the two cylinders in the back having a slightly reduced transfer. For N_{39} , the transfer from the front cylinders, $N_{39,(34-39)}$ (where the first subscript is the number of cylinders in the array and the second index refers to the i th cylinder; see Figures 6d–6f for location of cylinders), is well predicted. For cylinders in the middle and back of the array, the transfer is reduced (seen as a slight asymmetry in the polar plot in Figure 6b), and the theoretical predictions are consistently higher than the numerical simulations. Also, the prediction of the mathematical model is quite variable, which is due to the strong interaction between wakes of upstream cylinders for the cylinders at the back in this array. The cylinder at the front, $N_{39,36}$, does not have the highest mean transfer as the fluid decelerates immediately in front of the array due to the collective action of the cylinders ($\bar{Nu} = 9.4$ for $N_{39,36}$) and as the fluid accelerates around the sides, the cylinders with the highest mean Nusselt number are at approximately ± 60 degrees from the front of the array (e.g., $\bar{Nu} = 10$ for $N_{39,33}$) which can be seen in Figure 6b. The effect of the acceleration around the sides is more pronounced for N_{133} as the collective action of the cylinders is greater. For N_{133} the theoretical model slightly overpredicts the transfer from the front cylinders which is anticipated as the dipole/point force model underpredicts the deceleration in front of the array (Nicolle & Eames, 2011), resulting in an overprediction of the local Reynolds number and the subsequent transfer. For N_{133} , Figure 6c shows the dramatic reduction in scalar transfer of individual cylinders, from the front to the back of the array. For $Re = 333$, the array N_{39} has approximately the same group Nusselt number as N_{133} (see Figure 5b). However, it can be seen in Figures 6b and 6c that nearly all cylinders in N_{39} have an individual Nusselt number greater than 5, whereas no cylinders in the middle and back of the array N_{133} contribute to the mean group Nusselt number. It therefore remains to investigate the constituent reasons for individual cylinders having a modified transfer (compared to an isolated cylinder).

The analytical model can give a reasonable estimate for the mean transfer from the individual cylinders; however the numerical simulations are required to investigate the effect of the locally (un)steady incident (i) flow and (ii) passive scalar characteristics on the transfer from the cylinders. To this end, the front

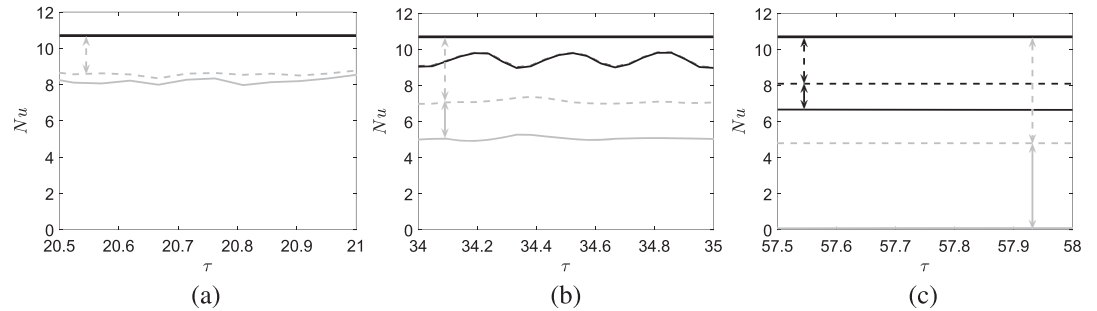


Figure 7. Time series showing the Nusselt number of individual cylinders at $Re = 333$ for (a) $N_{7,4}$ (gray lines), (b) $N_{39,19}$ (black lines) and $N_{39,26}$ (gray lines), and (c) $N_{133,90}$ (black lines) and $N_{133,106}$ (gray lines). Dashed and full lines indicate that $T = 0$ and $T = 1$ have been set on all other cylinders, respectively. The thick line represents the transfer for an isolated cylinder at $Re = 333$ ($\bar{Nu} = 10.7$). The difference between the thick line and the dashed line (given by the dashed double arrowed line) is the reduction in transfer due to the modification of the incident flow. The remainder is due to an incident flow with $T \neq 0$ (full double arrowed line). See Figures 6d–6f for location of cylinders.

and back cylinders of N_7 , N_{39} , and N_{133} for $Re = 333$ are considered in more detail. To differentiate between (i) and (ii) above, additional numerical simulations were carried out with $T = 0$ on all other cylinders while keeping $T = 1$ on the cylinder which was being investigated. In Figure 7, the difference between the thick line (which is the Nusselt number of an isolated cylinder) and the dashed line is the reduction in the transfer due to the modification of the incident flow and the difference between the dashed line and the full thin line is reduction due to the incident flow having a scalar value $T \neq 0$. As the solid fraction increases, for cylinders at the back of the array, the effect of the incident passive scalar becomes more important. For $N_{7,4}$, the effect of the incident passive scalar is small (Figure 7a), whereas the transfer from $N_{133,126}$ is close to zero with the two processes accounting for approximately 50% each of the reduction (Figure 7c). For cylinder $N_{39,19}$, the effect of the incident passive scalar is negligible. However, alternate vortex shedding from the upstream cylinders $N_{39,(36,37)}$, result in either an accelerated or decelerated flow around the upper or lower surface of the cylinder, leading to an oscillatory transfer ($Nu = 9.4 \pm 0.4$) seen in Figure 7b. The Strouhal number of this oscillation is 0.15 which is the same as that calculated for the lift force and the maximum of the Nusselt number is in phase with the maximum drag force on the cylinder. For comparison, the upstream cylinder ($N_{39,36}$) has a transfer of $\bar{Nu} = 9.4$ with nearly zero fluctuation as it is subjected to a uniform freestream while the cylinder $N_{39,33}$ has a transfer $Nu = 10 \pm 0.8$, as the flow is accelerated around the sides and it is sitting in the wake of $N_{39,34}$.

The overall effect is that, initially, as the number of cylinders increases the group transfer increases, as the interaction between the individual cylinders is weak. However, after a certain point, the collective action of all the cylinders results in cylinders having a significantly different transfer (compared to isolated cylinders), because (i) the modification of the incident flow on each cylinder and (ii) an incident flow with $T \neq 0$. Four processes in (i) have been identified in this work, namely, (a) deceleration in front of the array leading to a reduced transfer, (b) acceleration round the sides of the array leading to an enhanced transfer, (c) a fluctuating incident flow and (d) reduced local Reynolds number. (c) and (d) are due to a cylinder situated in the wakes of upstream cylinders. This results in the group transfer decreasing for higher solid fraction arrays.

6. Conclusions

In this work we have considered the effect of varying the Reynolds number and solid fraction on the transfer and transport of a passive scalar from an isolated array of circular cylinders, where the Reynolds number was chosen to reflect that found in aquatic canopies. As expected, the mean group transfer was found to increase as the Reynolds number was increased. However, when the solid fraction was increased, the group transfer increased, reached a maximum, and then decreased. This is due to the collective action of all the cylinders resulting in (i) a modification of the locally incident flow and (ii) a reduction in the scalar gradient between the cylinder surface and the incident flow on individual cylinders. To help interpret the numerical

results, a mathematical model was developed to estimate this transfer, which broadly included (i) and (ii) above. Agreement between the numerical simulations and the mathematical model were good. This work highlights the dramatic effect of solid fraction on the flow through an array, which will have important implications on the design of marine aquaculture. To make aquaculture a viable activity a certain density and infrastructure is required; however this needs to be balanced by adequate volume flux through the array to enable flushing of generated waste.

Appendix A: Validation of Numerical Method

In this section the numerical method is compared against the empirical correlations by Zhuauskas (1972)

$$\bar{Nu} = 0.51Re^{0.5}, \tag{A1}$$

and Knudsen and Katz (1958)

$$\bar{Nu} = 0.683Re^{0.466}Pr^{1/3}, \tag{A2}$$

in the literature (in addition to 9) and previous numerical simulations by Mahir and Altac (2014). The cases considered are shown in Table A1, which have been chosen as these cover all the scenarios present in the current numerical simulations. Figure A1a shows a mesh independence study of the mean Nusselt number for a cylinder at $Re = 200$ ($Pr = 0.7$). The choice of $\Delta/D = 0.02$ was chosen as the Nusselt number and the drag coefficient (not shown here) were within 1% for $Re = 100$ and 2% for $Re = 200$. For $Re = 333$, Δ/D had to be decreased to 0.01. Figure A1b shows the comparison of the local Nusselt number (for $Pr = 0.7$ and $Re = 200$) of the present simulations and those of Mahir and Altac (2014), where the angle is taken from the rear stagnation point. The global measure of the Nusselt number is compared in Table A1. It can be seen that agreement is good in all cases.

Table A1
The Mean Nusselt Number for an Isolated Circular Cylinder for the Current Simulations Compared With Previous Numerical Simulations and Empirical Correlations

Case	Re	Pr	Present	Mahir and Altac (2014)	(A1)	(A2)	(9)
1	100	0.7	5.19	5.179	5.10	5.19	5.16
2	200	0.7	7.54	7.47	7.21	7.16	7.19
3	100	1	5.95	—	5.0	5.84	5.89
4	333	1	10.7	—	9.12	10.23	10.57

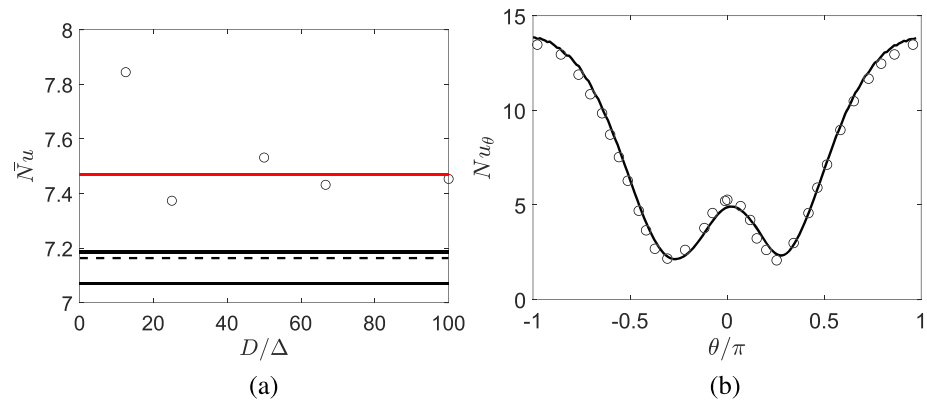


Figure A1. (a) Mesh independence study of the Nusselt number (for an isolated circular cylinder) where Δ is the resolution in the boundary layer for $Re = 200$ and $Pr = 0.7$. The thin, dashed, and thick lines represent the correlations for (A1), (A2), and (9), respectively. The red line is the numerical simulations by Mahir and Altac (2014). (b) Comparison of the local Nusselt number for $Re = 200$ and $Pr = 0.7$ between the present simulations (black line) and the numerical simulations of Mahir and Altac (2014) (o).

Data Availability Statement

Data and scripts to generate Figures 3, 4, and 6 can be found online (<https://doi.org/10.5522/04/12629918.v1>).

Acknowledgments

The author acknowledges the use of the UCL Grace and Kathleen High Performance Computing Facilities (Grace@UCL and Kathleen@UCL), and associated support services, in the completion of this work.

References

- Bannister, R. J., Johnsen, I. A., Hansen, P. K., Kutti, T., & Asplin, L. (2016). Near- and far-field dispersal modelling of organic waste from Atlantic salmon aquaculture in fjord system. *ICES Journal of Marine Science*, *73*, 2408–2419.
- Batchelor, G. K. (1967). *An introduction to fluid dynamics 1st edn*. Cambridge: Cambridge University Press.
- Belcher, S. E., Jerram, N., & Hunt, J. C. R. (2003). Adjustment of a turbulent boundary layer to a canopy of roughness elements. *Journal of Fluid Mechanics*, *488*, 369–398.
- Black, K. D. (2001). Mariculture, environmental, economic and social impacts of. *Encyclopedia Ocean Science*, *3*, 1578–1584.
- Chang, K., & Constantinescu, G. (2015). Numerical investigation of flow and turbulence structure through and around a circular array of rigid cylinders. *Journal of Fluid Mechanics*, *776*, 161–199.
- Chen, J. G., Zhou, T. M., Antonia, R. A., & Zhou, Y. (2017). Comparison between passive scalar and velocity fields in a turbulent cylinder wake. *Journal of Fluid Mechanics*, *813*, 667–694.
- Churchill, S. W., & Bernstein, M. J. (1977). A correlating equation for forced convection from gases and liquids to a circular cylinder in crossflow. *Journal of Heat and Mass Transfer*, *99*, 300–306.
- Clift, R., Grace, J., & Weber, M. E. (1978). *Bubbles droplets and particles*. Dover: Dover Publications.
- Davidson, M. J., Myline, K. R., Jones, C. D., Phillips, J. C., Perkins, R. J., Fung, J. C. H., & Hunt, J. C. R. (1995). Plume dispersion through large groups of obstacles—A field investigation. *Atmospheric Environment*, *29*, 3245–3256.
- Eames, I., Jonsson, C., & Johnson, P. B. (2011). The growth of a cylinder wake in turbulent flow. *Journal of Turbulence*, *12*, 1–16.
- Food and Agriculture Organization (2016). The state of world fisheries and aquaculture. FAO Fisheries and Aquaculture Department Food and Agriculture organization of the United Nations, Rome.
- Fischer, H. B., List, E. J., Koh, R. C. Y., Imberger, J., & Brooks, N. G. (1979). *Mixing in inland and coastal waters*. New York: Academic Press.
- Geuzaine, C., & Remacle, J.-F. (2009). Gmsh: A three-dimensional finite element mesh generator with built-in pre- and post-processing facilities. *International Journal for Numerical Methods in Engineering*, *79*, 1309–1331.
- Hinze, J. O. (1975). *Turbulence*. 1st edn. McGraw-Hill.
- Hunt, J. C. R., & Eames, I. (2002). The disappearance of laminar and turbulent wakes in complex flows. *Journal of Fluid Mechanics*, *471*, 111–132.
- Klettner, C. A., Eames, I., & Hunt, J. C. R. (2019). The effect of an unsteady flow incident on an array of circular cylinders. *Journal of Fluid Mechanics*, *872*, 560–593.
- Knudsen, J. D., & Katz, D. L. (1958). *Fluid dynamics and heat transfer*. New York: McGraw Hill.
- Koch, D. L., & Brady, J. F. (1986). The effective diffusivity of fibrous media. *AIChE Journal*, *32*, 575–591.
- Kumar, B., & Mittal, S. (2006). Effect of blockage on critical parameters for flow past a circular cylinder. *International Journal for Numerical Methods in Fluids*, *50*, 987–1001.
- Li, S., Katul, G., & Huai, W. (2019). Mean velocity and shear stress distribution in floating treatment wetlands: An analytical study. *Water Resources Research*, *55*, 6436–6449. <https://doi.org/10.1029/2019WR025131>
- Mahir, N., & Altac, Z. (2014). Numerical investigation of convective heat transfer in unsteady flow past two cylinders in tandem arrangements. *International Journal of Heat and Fluid Flow*, *29*, 1309–1318.
- Matsumura, M., & Antonia, R. A. (1993). Momentum and heat transport in the turbulent intermediate wake of a circular cylinder. *Journal of Fluid Mechanics*, *250*, 651–668.
- Nakamura, H., & Igarashi, T. (2004). Variation of Nusselt number with flow regimes behind a circular cylinder Reynolds numbers from 70 to 30000. *International Journal of Heat and Fluid Flow*, *47*, 5169–5173.
- Nepf, H. (1999). Drag, turbulence and diffusion in flow through emergent vegetation. *Water Resources Research*, *35*, 479–489.
- Nicolle, A., & Eames, I. (2011). Numerical study of flow through and around a circular array of cylinders. *Journal of Fluid Mechanics*, *679*, 1–31.
- Rajani, B. N., Kandasamy, A., & Majumdar, S. (2009). Numerical simulation of laminar flow past a circular cylinder. *Applied Mathematical Modelling*, *33*, 1228–1247.
- Rominger, J. T., & Nepf, H. M. (2011). Flow adjustment and interior flow associated with a rectangular porous obstruction. *Journal of Fluid Mechanics*, *680*, 636–659.
- Sumner, D. (2010). Two circular cylinders in cross-flow: A review. *Journal of Fluids and Structures*, *26*, 849–899.
- Taddei, S., Manes, C., & Ganapathisubramani, B. (2016). Characterisation of drag and wake properties of canopy patches immersed in turbulent boundary layers. *Journal of Fluid Mechanics*, *798*, 27–49.
- Tanino, Y., & Nepf, H. (2008). Lateral dispersion in random cylinder arrays at high Reynolds number. *Journal of Fluid Mechanics*, *600*, 339–371.
- Weller, H. G., Tabor, G., Jasak, H., & Fureby, C. (1998). A tensorial approach to computational continuum mechanics using object-oriented techniques. *Computers in Physics*, *12*, 620–631.
- White, B. L., & Nepf, H. (2003). Scalar transport in random cylinder arrays at moderate Reynolds number. *Journal of Fluid Mechanics*, *487*, 43–79.
- Wu, Y., Chaffey, J., Law, B., Greenberg, D. A., Drozdowski, A., Page, F., & Haigh, S. (2014). A three-dimensional hydrodynamic model for aquaculture: A case study in the Bay of Fundy. *Aquaculture Environment Interactions*, *5*, 235–248.
- Zhou, Y., Zhang, H. J., & Yiu, M. W. (2002). The turbulent wake of two side-by-side circular cylinders. *Journal of Fluid Mechanics*, *458*, 303–332.
- Zhuaskas, A. (1972). *Heat transfer from tubes in cross-flow advances in heat transfer*. New York: Academic Press.